International Symposium
On Turbulence and Shear Flow
Phenomena (TSFP-8)
August 28 - 30, 2013 Poitiers, France

NEW RESULTS ON THE STRUCTURE OF TURBULENCE IN A MIXING LAYER WITH AND WITHOUT SWIRL

Samuel Davoust, Laurent Jacquin and Benjamin Leclaire
Department of Fundamental and Experimental Aerodynamics
ONERA The French Aerospace Lab
F-92120, Meudon, France
laurent.jacquin@onera.fr

ABSTRACT

The near field of a 2.14×10^5 Reynolds number, low-Mach-number, cylindrical jet with and without swirl has been investigated by high-speed stereo PIV in a transverse plane, two diameters downstream of the jet exit. Using spatiotemporal correlations, we investigate the dynamics of streamwise vorticity in the shear layer, responsible for the mixing properties of the jet, and show how swirl affects this vorticity. A dynamical scenario is proposed, which explains how the mean shear and the azimuthal $m=0$ vortices contribute to the spatial organization observed.

INTRODUCTION

Organization of turbulence in a jet flow has remained an active field of research since early studies, due to the needs of accurate predictions in the fields of mixing, combustion and acoustics. In these applications, jets also often exhibit a degree of swirl, which may have a significant impact on this mixing. In past studies, the description, modelling and control of the large-scale structures in these jets have been recognized as major objectives. In the near field, the main dynamical features are known to be $m=0$ and $m=1$ oscillations of the jet column, along with streamwise vortical structures in the mixing layer and smaller-scale turbulence. Despite a large number of studies, the mechanism creating these vortices remains not fully determined, and also seems to be dependent to the Reynolds number and initial conditions. A detail physical understanding of the ability of swirl to enhance mixing also seems to be lacking. Our aim in this communication is to refine these views, in the case of a 2.14×10^5 Reynolds number, low-Mach-number, cylindrical jet, which may or not exhibit a large central zone of solid-body rotation. We measure the jet near field velocity by stereo PIV in longitudinal planes, and in a transverse plane located at two diameters from the exit. In this plane, the acquisition is performed at high frequency. We use these measurements to first characterize the evolution with swirl of the global mixing layer properties (spreading rate, maximum turbulent kinetic energy), and then to investigate in detail the dynamics of the coherent structures involved in the mixing process. We focus here in particular on the streamwise vortices, and their interaction with the $m=0$ modes. Finally, we propose dynamical scenarios which account for the origin and spatial structures of these vortices.

EXPERIMENTAL SETUP

Control parameters

We use an open return wind tunnel, which has been designed originally to study the effect of rotation on turbulence (Jacquin et al., 1990). In this facility, a centrifugal blower first drives the flow into a diffuser followed by a settling chamber. The flow then undergoes a first contraction from a 1 m square cross-section to a circular $D_c = 0.3m$ cross-section. As sketched in **Figure 1**, a 0.5 m long part of this cylindrical duct can be put into rotation with a controlled angular velocity Ω_c that can reach 1000 r.p.m . The rotating part contains a 0.1 m long honeycomb with 1.5 mm cell diameter. The jet, of exit diameter $D_0 = 0.15m$, is then generated by a contracting nozzle (contraction ratio $\chi = 4$, $L_c/D_c = 1.26$), ended by a 0.15 m long thin edged nozzle. The exit bulk velocity U_0 is defined by

$$U_0 = \frac{\dot{m}_0}{\rho\pi D_0^2/4} = \frac{\int_0^{0.5} u_z(z=0,r)\,r\,dr}{\int_0^{0.5} r\,dr}, \qquad (1)$$

where the exit flow rate $\dot{m}_0$ is kept constant thanks to a Venturi flow meter placed upstream of the fan air intake. The corresponding Reynolds number is

$$\mathrm{Re}_0 = \frac{U_0 D_0}{\nu} = 2.14\times10^5 \qquad (2)$$

In the sequel, U_0 and D_0 will be used to build dimensionless quantities. As far as rotation effects are concerned, the control parameter is the jet swirl number :

$$S_0 = \frac{\Omega_0 D_0/2}{U_0} \qquad (3)$$

where Ω_0 is the angular velocity of the exit flow. After contraction one has $\Omega_0 \approx \chi\Omega_c$ so that imposing the rotation rate Ω_c of the honeycomb amounts to control the flow conditions by means of the control swirl number :

$$S = \frac{\chi\Omega_c D_0/2}{U_0} \qquad (4)$$

The same was used by Liang and Maxworthy (2005). As shown by Leclaire and Jacquin (2012), the exit flow is in solid body rotation except for the boundary layers, and with a low axial turbulence level in the core (0.5 %), up to S = 0.81. This fixes the maximal swirl value considered in the present study.

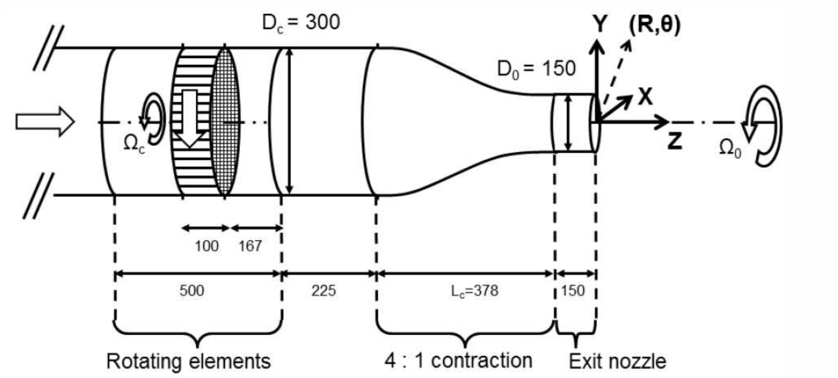

Figure 1 - Principle sketch of the swirling jet generation and frame of references. Dimensions are given in mm

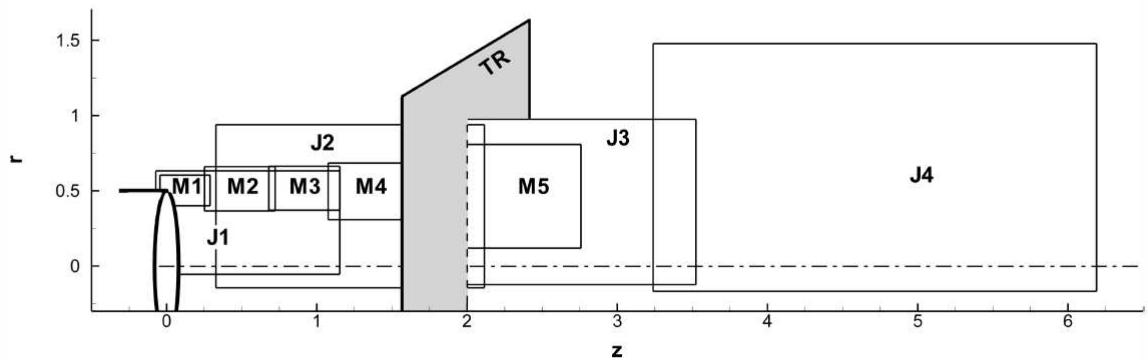

Figure 2 - Location of the PIV measurement planes performed. White planes identify conventional, low frame rate SPIV, and the gray plane high speed SPIV.

Measurements

We perform Stereo PIV (SPIV) performed in several planes, as shown in Figure 2. Longitudinal planes, labeled M1-M5 and J1-J4, correspond to a low frame rate, 4 Hz acquisition of N = 5000 samples per test. The z = 2 cross-sectional plane is investigated with High Speed SPIV (HS-SPIV). In this plane, 30 blocks of 2100 are acquired at 2.5 kHz for each measurement point. Calibration of the cameras is performed using a pin-hole model, and followed by a self-calibration as in Wieneke (2005) to correct any misalignment between the plate and the laser sheet.

Vector computation is performed using the ONERA in-house software FOLKI-SPIV, which is implemented on GPU (Champagnat et al, 2011) and uses a novel paradigm for Stereo PIV (Leclaire et al., 2012). In all cases, an interrogation window of 31x31 pixels is chosen to perform the image interrogation, corresponding to a variable spatial resolution depending on the PIV plane. Results are sampled every 13 pixels in the M1-M5 and J1-J4 planes (60 % overlap), and every 30 pixels in the HS-SPIV plane. In the latter case, this choice stems from the large amount of data involved. An uncertainty analysis shows that no significant peak-locking is present, and leads to an overall uncertainty of 0.3 $m.s^{-1}$, that is, 1.5 % of U_0. Further details, as well as the effect of spatial filtering especially in the HS-SPIV plane, can be found in Davoust et al. ,2012, and Davoust, 2012. In these studies, the sampling and post-processing were carefully validated against hot-wire measurements. The hot wire technique was also used to characterise the boundary layer in the exit plane of the nozzle.

EXIT FLOW CONDITIONS

The downstream evolution of the vorticity thickness, defined as

$$\delta_\omega = 1 \Big/ \left[-\frac{\partial u_z}{\partial r} \right]_{\max} , \tag{5}$$

and of the radial maximum of the turbulent kinetic energy k_m in the mixing layer) deduced form the J1 J2-J3 PIV planes measurements is shown in **Figure 3** for different swirl levels. One observes that the mixing layer growth rate is not a monotonic function of S : it slightly decreases for $S < 0.4$ and it is only for $S \geq 0.4$ that the unstable nature of the swirling mixing layer is clearly evidenced through δ_ω . This is due to changes in the contracting duct boundary layer with S , as revealed by the behaviour of k_m in **Figure 4(b)**. When swirl is added, it impacts both the boundary layer in the converging duct and the jet mixing layer. The impact of rotation on the boundary layer of the converging duct is a complex problem which lies out of the scope of the present paper.

As an illustration, **Figure 4** reveals that increasing S from 0 to 0.81 leads to non monotonous behaviours : the spreading rate of the mixing layer and the maximum value of the TKE of the incoming boundary layer (see **Figure 4(b)** for $z = 0.1$) decrease for $S < 0.4$ and increase for larger S . A non monotonic behaviour is also observed for the distance needed for stabilizing k_m : the leveling to a plateau of k_m is delayed downstream down to $z = 2$ for $S = 0.4$. Then, k_m reaches an asymptotic level for $z > 2$ close to $k_m = 0.4$ for $S = 0.2$ and

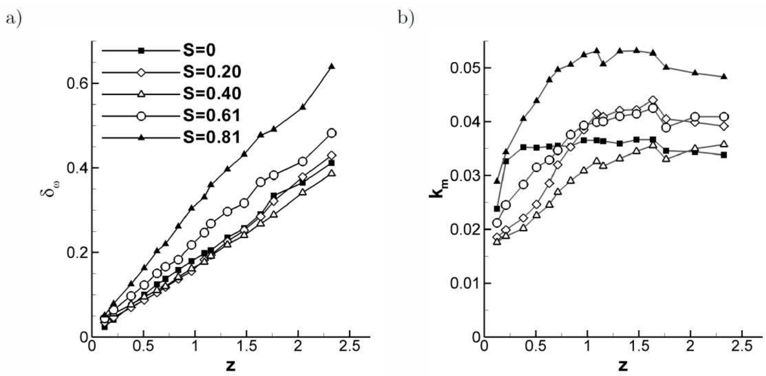

Figure 4 - Downstream evolution of vorticity thickness (a), and radial maximum of turbulent kinetic energy (b), for increasing swirl S.

$S = 0.61$, while $k_m \approx 0.5$ for $S = 0.81$. Cross flow velocity correlations show that the boundary layer is altered by Görtler like spatially coherent structures that appear for $S = 0.4$, see Davoust (2012). The wall bounded flow thus exhibits specific properties up to this particular value of S. Sensitivity to these changes in the initial conditions may propagate deeply downstream in the rotating mixing layer. For $S > 0.4$, rotation induced turbulence production mechanisms in the mixing layer dominate and lead to faster spatial growth of the mixing layer and to more energetic turbulence.
Consequently, the case $S = 0.61$, $z = 2$ has been selected here as one for which sensitivity to initial conditions has become weak enough, and where the structure of the mixing layer turbulence has reached a quasi-equilibrium state.

DYNAMICS OF COHERENT STRUCTURES

In this part, turbulence is studied from the point of view of its vortical organization. Streamwise oriented vortices will be especially considered as they are important dynamical features of shear flows, where they contribute actively to entrainment (Liepmann & Gharib 1992) and to Reynolds stresses (Nickels & Marusic 2001). Their role has been evidenced in fully turbulent axisymmetric mixing layers by Citriniti & George (2000) and by Davoust et al. (2011). This section describes in particular how swirl influences this streamwise vorticity.

Diagnosis tools

As noted by Rogers & Moin (1987), the two-point correlation of fluctuating vorticity components provides information on large scale vortical structures, while the vorticity fluctuation tensor $\langle \omega_i \omega_j \rangle$ describes small dissipative scales which dominate the vorticity spectrum. Our objective here is to provide a dynamical interpretation of the role of the largest vortical structures. This investigation is therefore based on the analysis of two point correlations of vorticity. Note that the Reynolds stresses can be theoretically recovered from the two point correlation of vorticity in spectral space, see Batchelor (1982). This means that the behavior of the Reynolds stress should be at least qualitatively described by that of the two-point correlation of vorticity. Using a method described in Davoust & Jacquin (2011) we have established that the validity of Taylor's hypothesis was degraded in the swirling jet compared to the non-swirling jet, mainly because of the increased turbulence levels and because the azimuthal component of the convection velocity could not be determined from the HS-SPIV measurement plane considered here. We therefore consider only the streamwise vorticity. For moderate swirl numbers, the large scale vorticity structures must remain fairly well described by this function, so let us consider the two-point correlation of the streamwise component of vorticity :

$$C_{\omega_z\omega_z}(r, r', \theta', t') = \frac{\langle \omega'_z(r,\theta,t)\,\omega'_z(r',\theta+\theta',t+t')\rangle_\theta}{\langle \omega'^2_z(r,\theta,t)\rangle_\theta} \qquad (6)$$

This function has been computed using a statistical average, noted $\langle\,\rangle_\theta$, which includes 210 independent data blocks and all the 128 azimuthal positions θ. At $r = 0.52$ the azimuthal integral angular scale is typically $20°$, so that the $\langle\,\rangle_\theta$ average is equivalent to nearly 2000 statistically independent samples. This provides a 95% confidence interval of ±0.04 with a normal distribution assumption (see Benedict & Gould 1996) upon estimating this $0 \le C_{\omega_z\omega_z} \le 1$ function. However, an investigation of the statistical symmetries that this function should verify for $S = 0$, leads to an even lower 95% confidence interval, i.e. rather ±0.004.

We restrict ourselves to the study of the statistical shape of vortical structures in the region where k is maximum, i.e. setting $r = 0.52$ in eq. (6).

Results

A time sequence acquired by HS-SPIV transformed into a pseudo-spatial sequence is shown in **Figure 5** for $S = 0$. This is obtained by introducing a reconstructed pseudo-axial coordinate, $z_c = -u_c t$, where $u_c = 0.6$ is a constant convection velocity as determined from Davoust & Jacquin (2011). Two different variables are characterized : the streamwise vorticity ω'_z (two opposite sign iso-surfaces) and the streamwise velocity fluctuation map at $r = 0.24$, that is in the non turbulent core of the jet. This pseudo-spatial sequence describes the local spatial aspect of turbulence near $z = 2$ in the mixing layer. One can see that streamwise-oriented vortical structures dominate the mixing layer. One also sees that the streamwise velocity fluctuations in the jet core are dominated by axisymmetric perturbations. This variable may thus be used as a good sensor of $m = 0$ modes (axisymmetric modes).

An example of iso-contours of $C_{\omega_z\omega_z}$ for $S = 0$ is plotted in **Figure 6 (b)**. Note that the time separation t

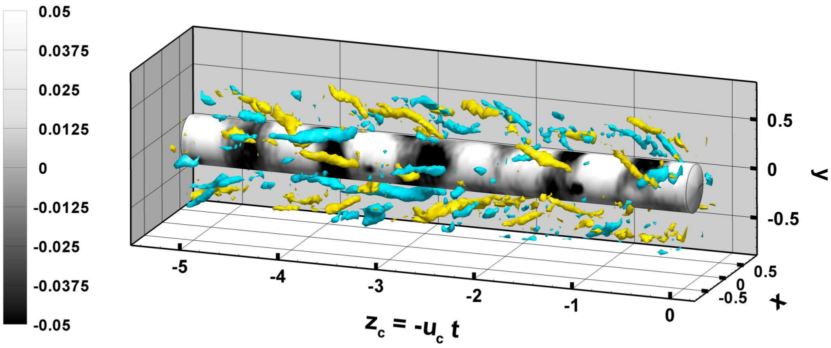

Figure 5 - Pseudo-spatial flow reconstruction along $z_c = -u_c t$ (arbitrary origin) from high speed SPIV data in the $z = 2$, using Taylor's hypothesis with $u_c = 0.6$. The streamwise velocity fluctuation $u_z^{'}$ at $r = 0.24$ is represented by grey contours. Yellow and blue iso-surfaces respectively identify $\omega_z^{'} = 4$ and -4 iso-values of the streamwise vorticity fluctuation.

has been replaced by the streamwise separation constructed with Taylor's hypothesis $z_c = -u_c t$, with $u_c = 0.6$, as above. No azimuthal convection velocity was used. One can see that $C_{\omega_z\omega_z}$ is a symmetric function of θ, consistent with the statistical invariance in azimuth. The patch of positive correlation centred around the probing point $(r'\theta' = 0, r' = r)$ exhibits a circular shape with a radius close to 0.1. This figure also reveals the existence of zones of negative $C_{\omega_z\omega_z}$ neighbouring this principal patch, indicating the occurrence of opposite-sign vorticity in the statistical sense. This leads to a global portrait featuring arrays of alternate-sign vortices, which are not preferentially distributed along the azimuth as depicted by Martin and Meiburg (1991) or Liepmann and Gharib (1992), among others, but rather along the radius. Further analysis, shown in Davoust et al. (2012), shows that a typical value of the inclination angle of these streamwise vortices in the longitudinal plane is roughly 20°. Rogers and Moin (1987) found a similar value in their DNS of homogeneous shear flow. When swirl is present, this inclination angle is found to be nearly independent on the value of S, i.e. still close to 20°. The effect of swirl is however more pronounced in the transverse plane. As shown in **Figure 6(c) to (f)**, a similar structure of the correlation iso-contours is observed, but with a global rotation around the probing point. As we will show below, this tilting may be ascribed to the change in the mean convection velocity due to swirl.

Dynamical scenarios

To account for the correlation structures observed in **Figure 6**, it is first useful to consider the relative magnitude of streamwise vorticity production mechanisms. Focusing on the $S = 0$ case for simplicity, streamwise vorticity may arise from two sources: the unsteady axial stretching from the $m = 0$ modes, and the steady stretching due to the mean shear of axial velocity. In the present experiment, as shown by Davoust et al. (2012), typical orders of magnitude show that the latter is predominant compared to the former. Indeed, the azimuthal vorticity perturbation conveyed by the $m = 0$ modes has been estimated to 0.6 thanks to a POD analysis, while a typical value for the mean shear of axial velocity is $1/\delta_\omega = 2.8$, where the vorticity thickness is $\delta_\omega = 0.36$. This predominance is confirmed by the fact that a typical value of the streamwise vorticity perturbation is 2.5, i.e. the same order of magnitude as the axial shear. Supplementary stretching by the unsteady $m = 0$ strain in fact acts as a partial spatial synchronization of the streamwise vortices in the so-called braid region, i.e. between two subsequent $m = 0$ rollers, as shown in Davoust et al. (2012). Such a synchronization can be observed in **Figure 5**, where the $m = 0$ modes are rather monitored by their signature in the core of the jet.

In order to explain the radial structure of opposite-sign streamwise vorticity observed in **Figure 6**, one now considers one of these vortices, in a frame of reference convected with the $m = 0$ structure, and taking this spatial synchronization into account (**Figure 7**, top left subfigure). Here this vortex is positive; using a negative one would lead to the same conclusions. As a consequence of the difference in magnitude between this vortex and the $m = 0$ modes highlighted above, the streamwise vortex tilts the negative $m = 0$ vorticity and produces radial vorticity fluctuations (top right). The mean shear then produces streamwise vorticity that has an opposite sign to the streamwise vortex considered, by tilting and stretching (bottom left). The ingredients of this mechanism are thus the mean shear associated with the streamwise velocity profile, the streamwise vortex, and the streamwise-periodic azimuthal vorticity, arising here from a pseudo-periodic instability mode, and may thus be at work in other situations where these features are present. Interestingly, evidence of a similar arrangement of opposite vorticity around streamwise vortices is indeed observed, though not discussed by the authors, in the plane mixing-layer simulation of Metcalfe et al. (1987), see their figure 19. We suspect that in past experiments, this organization could not be discriminated, as smoke flow visualizations were used, for which only the vorticity at the interface between marked and unmarked fluid is seen. Also, it may not have been detected in homogeneous turbulent shear flow, in which there is no periodically organized azimuthal (transverse) vorticity. When swirl is added, the rotation of the negative contours observed in **Figure 6** (right) can be explained by an additional mechanism, namely the differential convection by the mean azimuthal velocity. The tilting of the radial

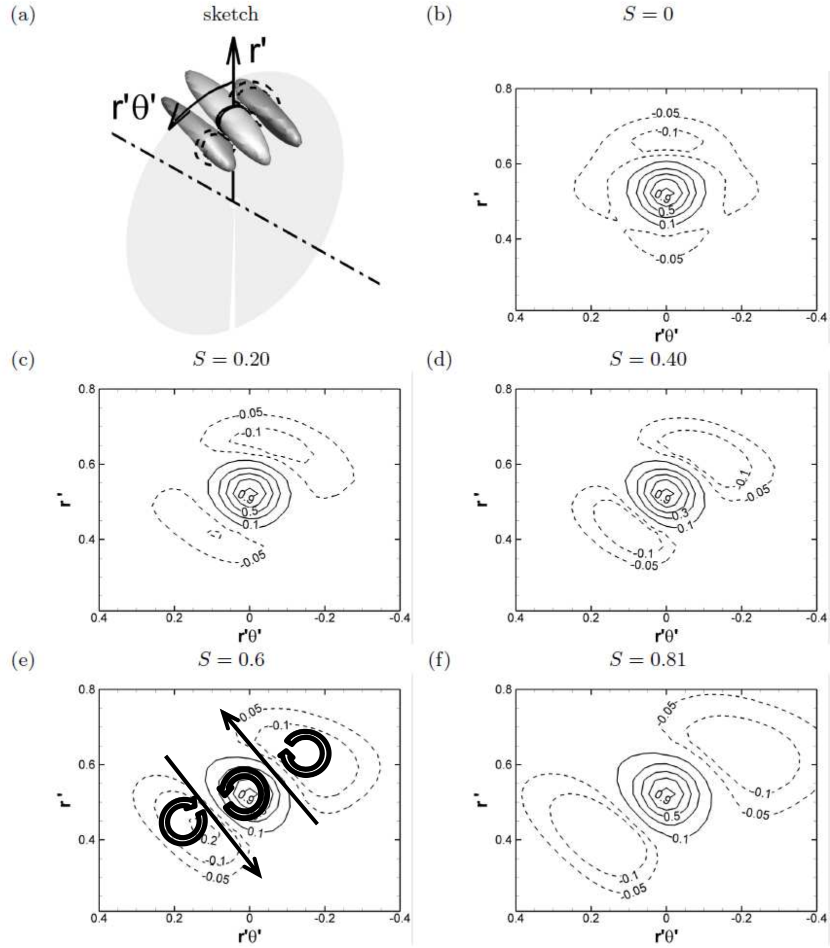

Figure 6 - Streamwise vorticity auto-correlation $C_{\omega_z\omega_z}$ defined in eq. (6). (a): Three-dimensional representation with a cut in $(r', r'\theta')$ cross-sections for $t' = 0$ and $S = 0.6$. In this plane, contours are shown for $S = 0$, (b), $S = 0.2$, (c), $S = 0.4$, (d), $S = 0.61$ (e) and $S = 0.81$ (f).

vorticity into streamwise vorticity occurs in the azimuthal direction, as depicted in **Figure 7** (bottom right), which explains the increasing tilting. As shown in **Figure 6** on the case $S = 0.6$ (bottom left) the kinematics induced by the tilted vortex tripole structure may then explain the increase in the radial mixing in a swirling mixing layer.

CONCLUSION

The mixing layer dynamics of a swirling and non swirling jet of exit Reynolds number equal to 2.14×10^5 has been characterized in several stereo PIV planes, with a specific attention to streamwise vorticity, mainly responsible for the jet mixing, and its interaction with the other jet dynamical features. Contrary to past studies, we evidenced that for $S = 0$, this vorticity exhibits a radially piled structure in a transverse plane, that is, *radial* arrays of alternate sign streamwise vortices, instead of the more usual *azimuthal* structure for these positive and negative vortices. As described in detail in Davoust et al. (2012) and exemplified here thanks to a pseudo-spatial 3D reconstruction using Taylor's hypothesis, these vortices are preferentially located between two subsequent $m = 0$ rollers. The addition of swirl in the jet results in a rotation around the jet axis of this structure, in an extent that depends on the swirl number. Using scaling arguments, we showed that the origin for the existence of streamwise vorticity in our jet is preferentially the steady stretching due to the mean shear of axial velocity, rather than the unsteady axial stretching from the $m = 0$ modes. In particular, the latter contain much less vorticity than the streamwise vortices. Finally, this led us to propose mechanisms explaining the spatial patterns observed for this streamwise vorticity in a transverse plane. At $S = 0$, the presence of negative streamwise vorticity patches above and below (in the radial sense) an initial positive streamwise vortex may in fact be a part of the $m = 0$ azimuthal vortices, firstly tilted by the positive streamwise vortex, and then tilted and stretched by the mean axial shear. In the presence of swirl, an additional tilting and stretching by the mean shear due to the azimuthal velocity component, may then account for the rotation observed for this structure.

REFERENCES

Batchelor, G.K., 1967, "An introduction to fluid dynamics". Cambridge Univ Pr, 1967.

Bradshaw, P., 1966, "The effect of initial conditions on the development of a free shear layer", *J. Fluid Mech.*, Vol. 26(02), pp.:225–236.

Benedict, L.H, Gould, R.D., 1996, "Towards better uncertainty estimates for turbulence statistics", *Exp. Fluids*, Vol. 22(2), pp. 129–136.

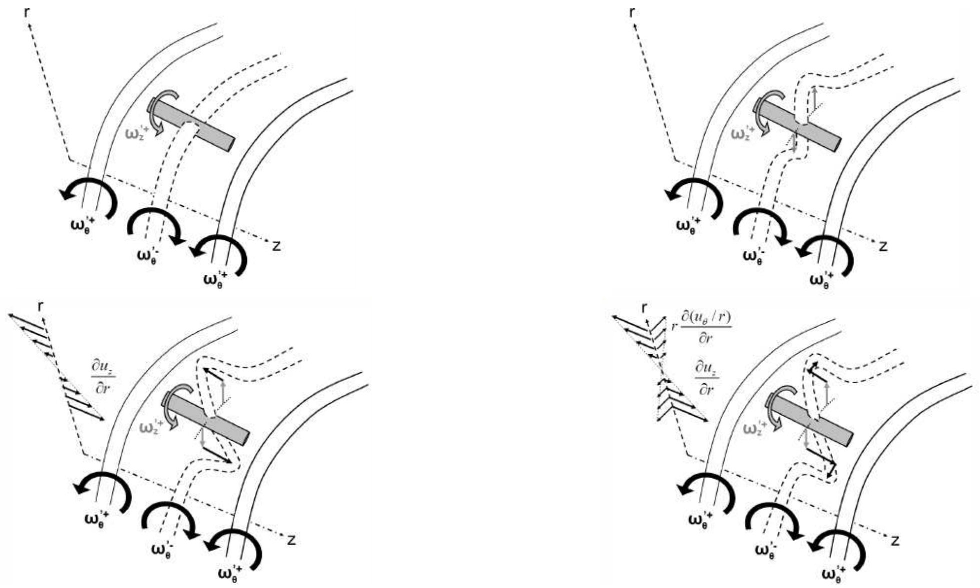

Figure 7 - Mechanism accounting for the generation of opposite-sign streamwise vorticity, derived from the present results. (top left): Initial most probable position of a streamwise vortex with respect to an $m=0$ mode. (top right): Tilting of the negative azimuthal vorticity of the $m=0$ mode by the streamwise vortex. (bottom left): tilting and stretching of the deformed ring by the mean shear, leading to the structure observed for $S=0$. (bottom right): the presence of swirl induces an additional tilting and stretching of the deformed ring by the mean shear (both axial and azimuthal).

Champagnat, F,. Plyer, A, Le Besnerais, G, Leclaire, B., Davoust, S. and Le Sant, Y, 2011, "Fast and accurate PIV computation using highly parallel iterative correlation maximization", *Exp. Fluids*, Vol. 50, pp. 1169-1182.

Davoust, S., and Jacquin, L., 2011, « Taylor's hypothesis convection velocities from mass conservation equation", *Phys. Fluids*, Vol. 23(5).

Davoust, S., Jacquin, L., and Leclaire, B., 2012, "Dynamics of m = 0 and m = 1 modes and of streamwise vortices in a turbulent axisymmetric mixing layer", *J. Fluid Mech.*, Vol. 709, pp. 408-444.

Davoust S., 2012, "Dynamique des grandes échelles dans les jets turbulents avec ou sans effets de rotation", Thèse de l'Ecole polytechnique.

Jacquin, L., Leuchter, O., Cambon, C. and Mathieu, J., 1990, "Homogeneous turbulence in the presence of rotation", *J. Fluid Mech.*, Vol. 220, pp. 1-52.

Leclaire, B. and Jacquin, L., 2012, "On the generation of swirling jets: high-Reynolds-number rotating flow in a pipe with a final contraction", *J. Fluid Mech.*, Vol. 692, pp. 78-111.

Leclaire, B., Parinet, S., Le Sant, Y., Champagnat, F. and Le Besnerais, G., 2012, "One-step stereo PIV: theory and performances", 16th Int Symp on Applications of Laser Techniques to Fluid Mechanics, Lisbon, Portugal, 09-12 July, 2012.

Liang, H., and Maxworthy, T., 2005, "An experimental investigation of swirling jets", *J. Fluid Mech.*, Vol. 525, pp. 115-159.

Liepmann, D., and Gharib, M., 1992, "The role of streamwise vorticity in the near-field entrainment of round jets", *J. Fluid Mech.*, Vol. 245, pp.643-668.

Martin, J. E., and Meiburg, E., 1991, "Numerical investigation of three-dimensionally evolving jets subject to axisymmetric and azimuthal perturbations", *J. Fluid Mech.*, Vol. 230, pp. 271-318.

Metcalfe, R. W., Orszag, S. A., Brachet, M. E., Menon, S. and Riley, J. J., 1987, "Secondary instability of a temporally growing mixing layer", *J. Fluid Mech.*, Vol. 184, pp. 207-243.

Rogers, M.M, and Moin, P., 1987, " The structure of the vorticity field in homogeneous turbulent flows", *J. Fluid Mech.*, Vol. 176, pp. 33–66.

Wieneke, B., 2005, "Stereo-PIV using self-calibration on particle images", *Exp. Fluids*, Vol. 39(2), pp. 267-280.